

Photoinduced η Pairing in the Hubbard Model

Tatsuya Kaneko¹, Tomonori Shirakawa^{2,1,3,4}, Sandro Sorella^{2,5,3}, and Seiji Yunoki^{1,3,4}

¹Computational Condensed Matter Physics Laboratory,

RIKEN Cluster for Pioneering Research (CPR), Wako, Saitama 351-0198, Japan

²SISSA–International School for Advanced Studies, Via Bonomea 265, 34136 Trieste, Italy

³Computational Materials Science Research Team,

RIKEN Center for Computational Science (R-CCS), Kobe, Hyogo 650-0047, Japan

⁴Computational Quantum Matter Research Team,

RIKEN Center for Emergent Matter Science (CEMS), Wako, Saitama 351-0198, Japan

⁵Democritos Simulation Center CNR–IOM Instituto Officina dei Materiali, Via Bonomea 265, 34136 Trieste, Italy

(Dated: February 26, 2019)

By employing unbiased numerical methods, we show that pulse irradiation can induce unconventional superconductivity even in the Mott insulator of the Hubbard model. The superconductivity found here in the photoexcited state is due to the η -pairing mechanism, characterized by staggered pair-density-wave oscillations in the off-diagonal long-range correlation, and is absent in the ground-state phase diagram; i.e., it is induced neither by a change of the effective interaction of the Hubbard model nor by simple photocarrier doping. Because of the selection rule, we show that the nonlinear optical response is essential to increase the number of η pairs and thus enhance the superconducting correlation in the photoexcited state. Our finding demonstrates that nonequilibrium many-body dynamics is an alternative pathway to access a new exotic quantum state that is absent in the ground-state phase diagram, and also provides an alternative mechanism for enhancing superconductivity.

Recent experiments have clearly demonstrated that nonequilibrium dynamics can induce many intriguing phenomena in condensed-matter materials [1–5]. Among them, the most striking is the discovery of photoinduced transient superconducting behaviors in some high- T_c cuprates [6–8] and alkali-doped fullerenes [9, 10]. It has also been theoretically shown that superconductivity can be enhanced or induced by pulse irradiation in models for these materials [11–14]. In these studies, the main focus is a photoinduced state with physical properties already present in the corresponding equilibrium phases. In the case of a Mott insulator (MI), photoinduced insulator-to-metal transitions have been reported in time-resolved experiments for several transition-metal and organic-molecular compounds [15–19]. In the MI, the photoinduced metallic state has been recognized as a result of photocarrier doping by creating doublon-holon pairs with no peculiar electronic states emerging [20–22].

In this Letter, we show that pulse irradiation can induce superconductivity even in the celebrated MI of the Hubbard model. The photoinduced superconductivity is due to the η -pairing mechanism, forming on-site singlet pairs that exhibit, unlike conventional s -wave superconductivity, the staggered off-diagonal long-range correlation with a phase of π . Because of the selection rule, the nonlinear optical response is essential to increasing the number of η pairs, and thus enhancing the superconducting correlation. Therefore, our finding is distinct from the previous studies [23–26] and provides an alternative mechanism for enhancing superconductivity via nonequilibrium dynamics.

To demonstrate that superconductivity can be photoinduced in a MI, here we consider the half-filled one-dimensional (1D) Hubbard model at zero temperature. However, our finding does not depend on spatial dimen-

sionality [26]. The model is described by the following Hamiltonian:

$$\hat{\mathcal{H}} = -t_h \sum_{i,\sigma} \left(\hat{c}_{i,\sigma}^\dagger \hat{c}_{i+1,\sigma} + \text{H.c.} \right) + U \sum_i \hat{n}_{i,\uparrow} \hat{n}_{i,\downarrow}, \quad (1)$$

where $\hat{c}_{i,\sigma}$ ($\hat{c}_{i,\sigma}^\dagger$) is the annihilation (creation) operator for an electron at site i with spin σ ($=\uparrow, \downarrow$) and $\hat{n}_{i,\sigma} = \hat{c}_{i,\sigma}^\dagger \hat{c}_{i,\sigma}$. t_h is the hopping integral between the nearest-neighboring sites, while U (> 0) is the on-site repulsive interaction. At half-filling, the ground state (GS) of the repulsive 1D Hubbard model is the MI with strong antiferromagnetic correlations.

A time-dependent external field is introduced via the Peierls phase in Eq. (1) by replacing $t_h \hat{c}_{i,\sigma}^\dagger \hat{c}_{i+1,\sigma} \rightarrow t_h e^{iA(t)} \hat{c}_{i,\sigma}^\dagger \hat{c}_{i+1,\sigma}$ [36], where $A(t)$ is the vector potential as a function of time t , and the light velocity c , the elementary charge e , the Planck constant \hbar , and the lattice constant are set to 1. We consider a pump pulse given as $A(t) = A_0 e^{-(t-t_0)^2/(2\sigma_p^2)} \cos[\omega_p(t-t_0)]$ with the amplitude A_0 , the frequency ω_p , and the pulse width σ_p centered at time t_0 (> 0) [37–41]. With finite $A(t)$, the Hamiltonian becomes time dependent, $\hat{\mathcal{H}} \rightarrow \hat{\mathcal{H}}(t)$, and the equilibrium GS of $\hat{\mathcal{H}}$ at $t = 0$ evolves in time, indicated here by $|\Psi(t)\rangle$. We employ the time-dependent exact diagonalization (ED) method for a finite-size cluster of L (even) sites with periodic boundary conditions (PBC) to solve the time-dependent Schrödinger equation [26]. We set t_h (t_h^{-1}) as a unit of energy (time) and the total number N of electrons to be L at half-filling.

Enhancement of the double occupancy $n_d(t) = \frac{1}{L} \sum_i \langle \Psi(t) | \hat{n}_{i,\uparrow} \hat{n}_{i,\downarrow} | \Psi(t) \rangle$ has been already reported in photoexcited states of the MIs [40, 42–44]. Here, we find a significant increase of the superconducting pair cor-

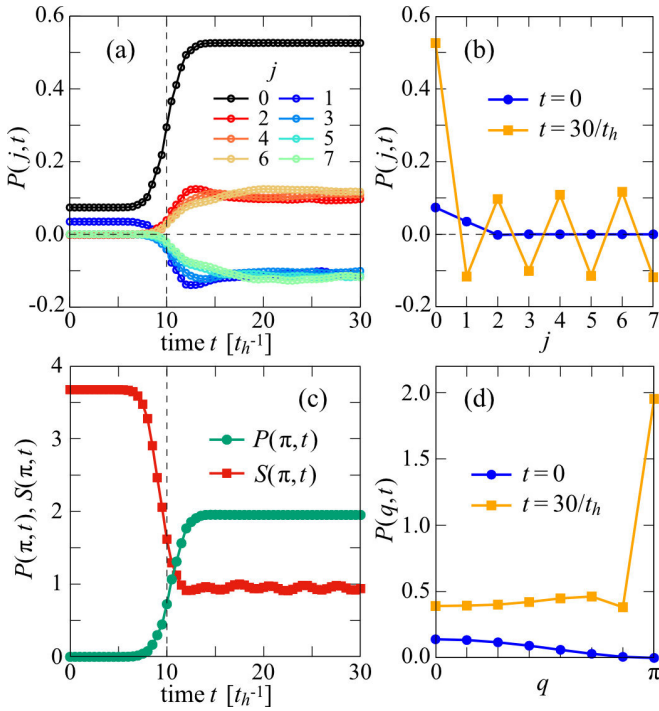


Figure 1. (a) Time evolution of the on-site pair-correlation function $P(j,t)$. (b) $P(j,t)$ at $t = 0$ and $30/t_h$. (c) Time evolution of the pair structure factor $P(q,t)$ and the spin structure factor $S(q,t)$ at $q = \pi$. (d) $P(q,t)$ at $t = 0$ and $30/t_h$. The results are calculated by the ED method for $L = 14$ at $U = 8t_h$ with $A_0 = 0.4$, $\omega_p = 8.2t_h$, $\sigma_p = 2/t_h$, and $t_0 = 10/t_h$.

relation for the on-site singlet pair $\hat{\Delta}_i = \hat{c}_{i,\uparrow}\hat{c}_{i,\downarrow}$ after the pulse irradiation. Figure 1(a) shows the time evolution of the real-space pair-correlation function defined as $P(j,t) = \frac{1}{L} \sum_i \langle \Psi(t) | (\hat{\Delta}_{i+j}^\dagger \hat{\Delta}_i + \text{H.c.}) | \Psi(t) \rangle$. Notice that $P(j,t)$ at $j = 0$ corresponds to the double occupancy, i.e., $P(j=0,t) = 2n_d(t)$. We thus confirm the enhancement of $n_d(t)$ by the pulse irradiation. Surprisingly, $P(j \neq 0,t)$ is also enhanced significantly by the pulse irradiation and oscillates with the opposite phases between odd and even sites.

As shown in Fig. 1(b), the pair correlation after the pulse irradiation extends to longer distances over the cluster, while the pair correlation is essentially absent in the initial MI state before the pulse irradiation. It is also clear that the sign of $P(j,t)$ alternates between neighboring sites, similar to a density wave, and accordingly the pair structure factor $P(q,t) = \sum_j e^{iqR_j} P(j,t)$, where R_j is the location of site j , shows a sharp peak at $q = \pi$ [see Fig. 1(d)]. The time evolution of $P(q,t)$ and the spin structure factor $S(q,t) = \sum_j e^{iqR_j} S(j,t)$, where $S(j,t) = \frac{1}{L} \sum_i \langle \Psi(t) | \hat{m}_{i+j}^z \hat{m}_i^z | \Psi(t) \rangle$ and $\hat{m}_i^z = \hat{n}_{i,\uparrow} - \hat{n}_{i,\downarrow}$, is also calculated at $q = \pi$ in Fig. 1(c). The antiferromagnetic correlation $S(q = \pi,t)$ is suppressed by the pulse irradiation, while the pair correlation $P(q = \pi,t)$ is

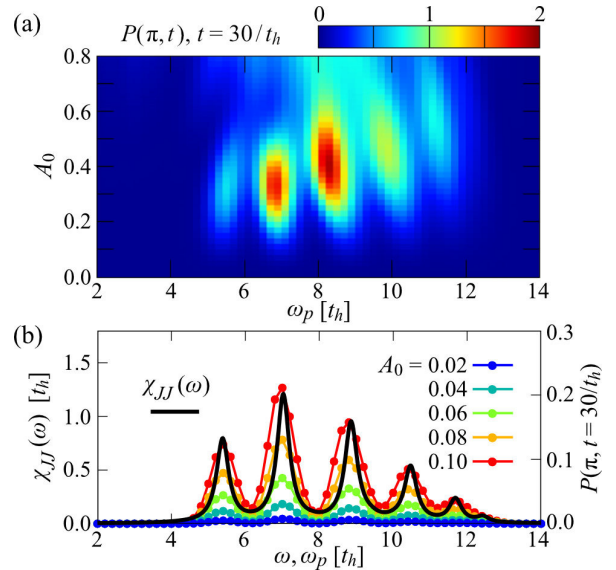


Figure 2. (a) Contour plot of the pair structure factor $P(q = \pi,t)$ at $t = 30/t_h$ with varying ω_p and A_0 . (b) The GS optical spectrum $\chi_{JJ}(\omega)$ is compared with $P(q = \pi,t = 30/t_h)$ as a function of ω_p for different values of A_0 . The results are calculated by the ED method for $L = 14$ at $U = 8t_h$, with $\sigma_p = 2/t_h$ and $t_0 = 10/t_h$.

strongly enhanced despite the fact that it is exactly zero before the pulse irradiation. Our matrix product state calculations also find the large enhancement of the pair correlation even for larger clusters that cannot be treated by the ED method [26].

In order to identify the optimal control parameters for the enhancement of $P(q = \pi,t)$, Fig. 2(a) shows the contour plot of $P(\pi,t)$ after the pulse irradiation with different values of A_0 and ω_p . For small A_0 , we find that the peak structure of $P(q = \pi,t)$ as a function of ω_p is essentially the same as the GS optical spectrum $\chi_{JJ}(\omega) = \frac{1}{L} \langle \psi_0 | \hat{J} \delta(\omega - \hat{\mathcal{H}} + E_0) \hat{J} | \psi_0 \rangle$, where $|\psi_0\rangle$ is the GS of $\hat{\mathcal{H}}$ with its energy E_0 and $\hat{J} = it_h \sum_{i,\sigma} (\hat{c}_{i+1,\sigma}^\dagger \hat{c}_{i,\sigma} - \hat{c}_{i,\sigma}^\dagger \hat{c}_{i+1,\sigma})$ is the current operator [see Fig. 2(b)]. This agreement is highly nontrivial and the reason will be clear below. $P(q = \pi,t)$ after the pulse irradiation is the largest at $A_0 \sim 0.4$ and $\omega_p \sim 8t_h$ ($= U$). We should emphasize that the enhancement of $P(q = \pi,t)$ cannot be explained simply by the photodoping of carriers into the MI or due to a dynamical phase transition induced by effectively varying the model parameters, because there is no region in the GS phase diagram of the Hubbard model showing large on-site pairing correlations.

Instead, the behavior of the on-site pairs in the photoinduced state shown in Fig. 1 can be understood in terms of the so-called η -pairing, a concept originally introduced by Yang [45]. In order to define the η -pairing, let us first introduce the following operators: $\hat{\eta}_j^+ = (-1)^j \hat{c}_{j,\downarrow}^\dagger \hat{c}_{j,\uparrow}^\dagger$, $\hat{\eta}_j^- = (-1)^j \hat{c}_{j,\uparrow} \hat{c}_{j,\downarrow}$, and $\hat{\eta}_j^z =$

$\frac{1}{2}(\hat{n}_{j,\uparrow} + \hat{n}_{j,\downarrow} - 1)$. Notice that $\hat{\eta}_j^+$ ($\hat{\eta}_j^-$) is the same as $\hat{\Delta}_j$ ($\hat{\Delta}_j$) except for the phase factor. These operators satisfy the $SU(2)$ commutation relations, i.e., $[\hat{\eta}_j^+, \hat{\eta}_j^-] = 2\hat{\eta}_j^z$ and $[\hat{\eta}_j^z, \hat{\eta}_j^\pm] = \pm\hat{\eta}_j^\pm$. Similarly, the total $\hat{\eta}$ operators, $\hat{\eta}^\pm = \sum_j \hat{\eta}_j^\pm$ and $\hat{\eta}_z = \sum_j \hat{\eta}_j^z$, satisfy the $SU(2)$ commutation relations. The essential property of the $\hat{\eta}$ operators here is that they also satisfy $[\hat{\mathcal{H}}, \hat{\eta}^\pm] = \pm U \hat{\eta}^\pm$ with $\hat{\mathcal{H}}$ in Eq. (1).

Yang originally proposed the η -pairing state $|\phi_{N_\eta}\rangle \propto (\hat{\eta}^+)^{N_\eta} |0\rangle$, where $|0\rangle$ is a vacuum with no electrons and N_η is the number of η pairs [45]. Yang's η -pairing state $|\phi_{N_\eta}\rangle$ has two remarkable properties [45]: First, $|\phi_{N_\eta}\rangle$ is an exact eigenstate of the Hubbard model with $2N_\eta$ electrons, satisfying $\hat{\mathcal{H}}|\phi_{N_\eta}\rangle = N_\eta U |\phi_{N_\eta}\rangle$. Second, $\langle\phi_{N_\eta}|\hat{\Delta}_i^\dagger \hat{\Delta}_j|\phi_{N_\eta}\rangle = \frac{N_\eta(L-N_\eta)}{L(L-1)} e^{i\pi(R_i-R_j)}$ for $i \neq j$, indicating that $|\phi_{N_\eta}\rangle$ exhibits off-diagonal long-range order. Notice that both Yang's η -pairing state $|\phi_{N_\eta}\rangle$ and our photoinduced state $|\Psi(t)\rangle$ show similar sign-alternating characters in the pair-correlation function. However, the photoinduced state $|\Psi(t)\rangle$ excited from the MI state is different from the η -pairing state $|\phi_{N_\eta}\rangle$, in which all electrons participate in forming η pairs, because we find numerically that $|\langle\phi_{N_\eta}|\Psi(t)\rangle|^2 = 0$ at $t = 30/t_h$.

As a candidate of the photoinduced state showing large $P(q = \pi, t)$, we now consider the eigenstate generated from the lowest-weight state (LWS) for $\hat{\eta}$ operators. For this purpose, it is important to notice that $[\hat{\mathcal{H}}, \hat{\eta}^+ \hat{\eta}^-] = [\hat{\mathcal{H}}, \hat{\eta}_z] = 0$. Therefore, any eigenstate of $\hat{\mathcal{H}}$ is also the eigenstate $|\eta, \eta_z\rangle$ of $\hat{\eta}^2$ and $\hat{\eta}_z$ with the eigenvalues $\eta(\eta+1)$ and η_z , respectively, where $\hat{\eta}^2 = \frac{1}{2}(\hat{\eta}^+ \hat{\eta}^- + \hat{\eta}^- \hat{\eta}^+) + \hat{\eta}_z^2$, $\eta = 0, 1, 2, \dots, \frac{L}{2}$ (at half-filling with the same number of up and down electrons $N_\uparrow = N_\downarrow$), and $\eta_z = -\eta, -\eta+1, \dots, \eta$. This is precisely the analogue to the total spin operator \hat{S} and its z component \hat{S}_z characterizing any eigenstate of $\hat{\mathcal{H}}$ with $|S, S_z\rangle_{\text{spin}}$. The LWS is $|\eta, \eta_z = -\eta\rangle$ and thus satisfies $\hat{\eta}^-|\eta, -\eta\rangle = 0$. Remarkably, Essler *et al.* have shown analytically that all the regular Bethe ansatz eigenstates of the 1D Hubbard model are the LWSs, and the remaining eigenstates can be generated from the LWSs by applying $\hat{\eta}^+$ [46–48].

Following them, we can construct the eigenstate having N_η η pairs from the LWS with $N_\uparrow = N_\downarrow = N_0$ ($\leq L/2$) as $|\psi_{N_\eta}\rangle = \frac{1}{\sqrt{C_{N_\eta}}}(\hat{\eta}^+)^{N_\eta}|\eta = \frac{L}{2} - N_0, \eta_z = -\eta\rangle$ [49].

Yang's η -pairing state $|\phi_{N_\eta}\rangle$ corresponds to $|\psi_{N_\eta}\rangle$ generated from the vacuum state with $N_0 = 0$. At half-filling, $|\psi_{N_\eta}\rangle$ should contain L electrons, and thus we consider $|\psi_{N_\eta}\rangle$ with $N_0 = L/2 - N_\eta$. Therefore, in this case, $|\psi_{N_\eta}\rangle \propto |\eta = N_\eta, \eta_z = 0\rangle$, and hence $\langle\psi_{N_\eta}|\hat{\eta}^+ \hat{\eta}^-|\psi_{N_\eta}\rangle = N_\eta(N_\eta + 1)$.

As an example, we construct $|\psi_{N_\eta}\rangle$ from the ground state $|\psi_{N_\uparrow, N_\downarrow}^{(\text{GS})}\rangle$ of $\hat{\mathcal{H}}$ with $N_\uparrow = N_\downarrow = N_0$ [51], which is the LWS. Figure 3 shows the on-site pair correlation, $P(j)$ and $P(q)$, for $|\psi_{N_\eta}\rangle$ with different N_η 's generated from $|\psi_{N_0, N_0}^{(\text{GS})}\rangle$. The sign-alternating character in $P(j)$ and the

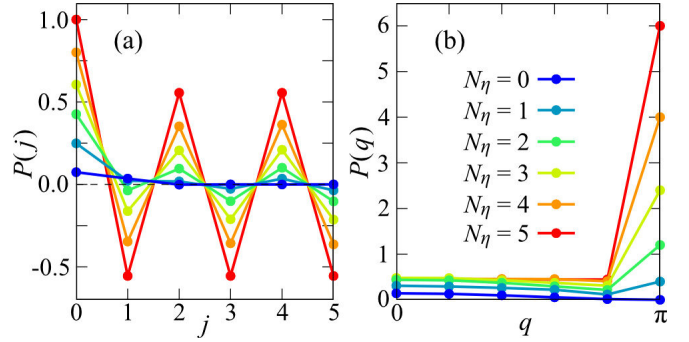


Figure 3. (a) On-site pair-correlation function $P(j)$ and (b) structure factor $P(q)$ for $|\psi_{N_\eta}\rangle$ at $U = 8t_h$ with the different number of η pairs N_η ($\leq L/2$). $|\psi_{N_\eta}\rangle$ is generated from the ground state $|\psi_{N_0, N_0}^{(\text{GS})}\rangle$ of $\hat{\mathcal{H}}$ with $N_0 = L/2 - N_\eta$ calculated by the ED for $L = 10$ under PBC.

enhancement of $P(q = \pi)$ are clearly observed. This is understood because $P(q = \pi) = 2\langle\psi_{N_\eta}|\hat{\eta}^+ \hat{\eta}^-|\psi_{N_\eta}\rangle/L = 2N_\eta(N_\eta + 1)/L$. With increasing N_η , $|\psi_{N_\eta}\rangle$ crossovers to Yang's η -pairing state $|\phi_{N_\eta=L/2}\rangle$ at $N_\eta = L/2$, for which $P(q = \pi)$ is the largest.

To elucidate the nature of the photoinduced state $|\Psi(t)\rangle$ in terms of the η pairs, we calculate the eigenenergies ε_m and the structure factors $P(q = \pi)$ for all the eigenstates $|\psi_m\rangle$ of $\hat{\mathcal{H}}$ at half-filling. As shown in Fig. 4(a), the structure factor $P(q = \pi)$ for each eigenstate is nicely quantized. This is because each eigenstate $|\psi_m\rangle$ is also the eigenstate of $\hat{\eta}^2$ and $\hat{\eta}_z$, and the quantized values are given as $P(q = \pi) = 2\langle\psi_m|\hat{\eta}^+ \hat{\eta}^-|\psi_m\rangle/L = 2\eta(\eta + 1)/L$, with $\eta = 0, 1, \dots, \frac{L}{2}$, corresponding to the number of η pairs. These quantized values are exactly the same as $P(q = \pi)$ calculated for $|\psi_{N_\eta}\rangle$ in Fig. 3(b).

In Fig. 4(a), the color of each point indicates the weight $|\langle\psi_m|\Psi(t)\rangle|^2$ of the eigenstate $|\psi_m\rangle$ in the photoinduced state $|\Psi(t)\rangle$ that exhibits the strong enhancement of $P(q = \pi, t)$ after the pulse irradiation [see the inset of Fig. 4(a)]. We find that the state $|\Psi(t)\rangle$ after the pulse irradiation contains the nonzero weights of the eigenstates $|\psi_m\rangle$ with finite η [also see Fig. 4(b)]. This is exactly the reason for the photoinduced enhancement of $P(q = \pi, t)$. The Hubbard model itself has the eigenstates with $P(q = \pi) \neq 0$, and the photoinduced state $|\Psi(t)\rangle$ captures the weights of those eigenstates.

The process of the enhancement of $P(\pi, t)$ is explained as follows: Before the pulse irradiation, the initial state is the GS of $\hat{\mathcal{H}}$ with $|\eta = 0, \eta_z = 0\rangle$, i.e., the η singlet state [48], and $P(q = \pi) = 0$. The pulse irradiation via $A(t)$ breaks the commutation relation as $[\hat{\mathcal{H}}(t), \hat{\eta}^+] = [\hat{\mathcal{H}}, \hat{\eta}^+] + \sum_k F(k, t) \hat{c}_{\pi-k,\downarrow}^\dagger \hat{c}_{k,\uparrow}^\dagger$, with $F(k, t) = 4t_h \sin[A(t)] \sin k$, and this transient breaking of the η symmetry stirs states with different values of η . After the pulse irradiation, the Hamiltonian again satisfies the commutation relation because $A(t) = 0$, but $|\Psi(t)\rangle$ now contains components of $|\eta \neq 0, \eta_z = 0\rangle$, which

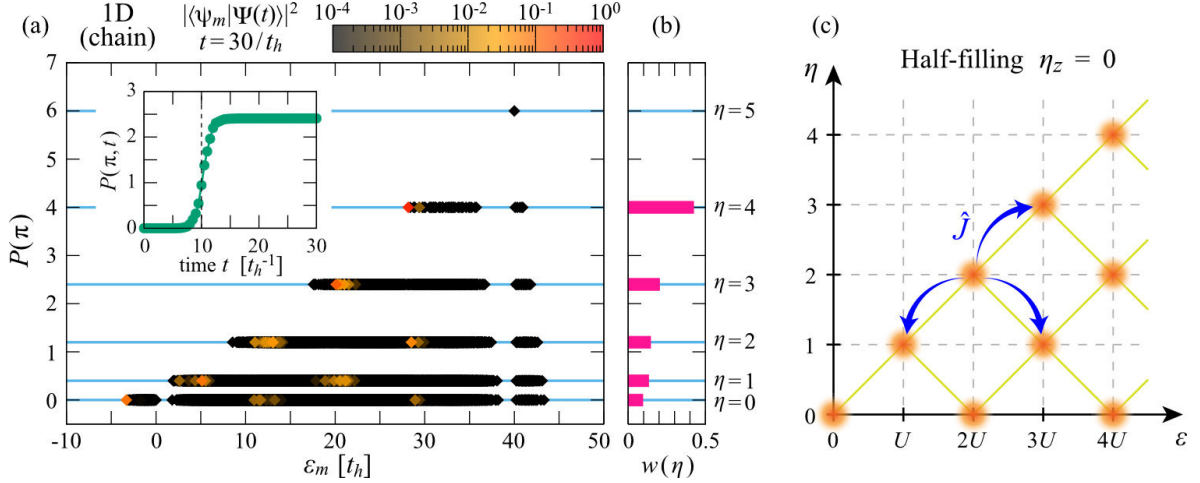


Figure 4. (a) All eigenenergies ε_m and $P(\pi)$ for the eigenstates $|\psi_m\rangle$ of the half-filled Hubbard Hamiltonian \hat{H} at $U = 8t_h$ and $L = 10$ under PBC. The color of each point indicates the weight $|\langle\psi_m|\Psi(t)\rangle|^2$ of the eigenstate $|\psi_m\rangle$ in the photoinduced state $|\Psi(t)\rangle$ at $t = 30/t_h$ for $A(t)$ with $A_0 = 0.4$, $\omega_p = 7.8t_h$, $\sigma_p = 2/t_h$, and $t_0 = 10/t_h$. The inset shows the time evolution of $P(\pi, t)$ for $|\Psi(t)\rangle$. (b) The total weight $w(\eta)$ of $|\langle\psi_m|\Psi(t)\rangle|^2$ over the states $|\psi_m\rangle$ with the same number η of η pairs in (a). Note that $\sum_{\eta=0}^{L/2} w(\eta) = 1$. (c) Schematic figure of a ‘tower of states’ $|\psi_m\rangle$ in the photoinduced state $|\Psi(t)\rangle$. The initial state before the pulse irradiation is at $(\varepsilon, \eta) = (0, 0)$. The current operator \hat{J} can induce the transition between states with $\Delta\eta = \pm 1$ and $\Delta\varepsilon \sim \pm U$, as indicated by arrows, assuming that $\omega_p \sim U$, and thus the pulse irradiation eventually excites a series of states with nonzero η and ε (indicated by orange spheres).

enhance $P(\pi, t)$.

More precisely, in the small- A_0 limit, the external perturbation is expressed as $A(t)\hat{J}$. We can show that the current operator \hat{J} is a rank-one tensor operator with the zeroth component in terms of the $\hat{\eta}$ operators [26]. Therefore, according to the Wigner-Eckart theorem [52], there exists the selection rule such that $\langle\eta', \eta'_z| \hat{J} |\eta, \eta_z\rangle \neq 0$ only for $\eta' = \eta \pm 1$ when $\eta'_z = \eta_z = 0$ at half-filling. This implies that in the linear response regime the photoinduced state $|\Psi(t)\rangle$ can contain the eigenstates $|\psi_m\rangle$ with $\eta = 1$ and the eigenenergies $\varepsilon_m \sim U$, assuming that ω_p is tuned around U . This explains the good agreement between the optical spectrum $\chi_{JJ}(\omega)$ and $P(q = \pi, t)$ found in Fig. 2(b). At the second order, the photoinduced state $|\Psi(t)\rangle$ can contain eigenstates $|\psi_m\rangle$ of \hat{H} with $\eta = 2$ and $\varepsilon_m \sim 2U$, as well as $\eta = 0$ and $\varepsilon_m \sim 0$ and $2U$. Applying the same argument for higher orders, η -pairing eigenstates with even larger η values acquire in the transient period a finite overlap $|\langle\psi_m|\Psi(t)\rangle|^2$ with the photoinduced state. Considering all orders, eventually, the distribution of eigenstates $|\psi_m\rangle$ in the photoinduced state $|\Psi(t)\rangle$ forms a ‘tower of states’ shown schematically in Fig. 4(c), which is indeed in good qualitative accordance with the numerical results in Fig. 4(a) (for the analysis in the limit of $\sigma_p \rightarrow \infty$, see the Supplemental Material [26]). This also explains why the pulse irradiation is effective to induce η pairs, and the nonlinearity is essential to enhance the pair correlation. Note that the nonlinear response is absent in the noninteracting limit, clearly showing the importance of electron correlations.

Exactly the same argument can be applied to the two-

dimensional Hubbard model on the square lattice, and indeed we have found the large enhancement of the on-site pairing correlation in the photoinduced state, similar to the 1D case [26]. Although the enhancement of the pair correlation is most effective at half-filling, it remains even away from half-filling [26]. We have also examined the effect of perturbation \hat{H}' that breaks the η symmetry, i.e., $[\hat{H}', \hat{\eta}^+ \hat{\eta}^-] \neq 0$, and still found the enhancement of the η -pairing correlation specially in the transient period [26].

In conclusion, we have found that density-wave-like staggered superconducting correlations are induced by photoexciting the MI ground state of the half-filled Hubbard model. The superconductivity is due to the η -pairing mechanism where the on-site singlet pairs display off-diagonal long-range correlation with phase π , the fingerprint of the η -pairing state. We have shown that the nonlinear optical response is essential to increase the number of η pairs and hence enhance the superconducting correlation. The η -pairing states were originally introduced purely for the mathematical purpose to solve the Hubbard model analytically, and here we have demonstrated that the pulse irradiation can bring this object into the real world to be observed experimentally.

Finally, we note that a more realistic treatment of materials should include a coupling with other degrees of freedom such as phonons, which introduces slow timescale dynamics in the thermalization process. Therefore, the η -pairing may be realized experimentally in a transient or prethermal regime. The most ideal system to explore the η -pairing experimentally is a cold fermionic

atom system, for which the antiferromagnetic order has been recently observed [53].

The authors acknowledge S. Sota, K. Seki, S. Miyakoshi, T. Oka, S. Kitamura, P. Werner, Y. Murakami, and S. Ishihara for fruitful discussion. This work was supported in part by Grants-in-Aid for Scientific Research from MEXT Japan under Grants No. JP17K05523, No. JP18K13509, and No. JP18H01183. T. S. acknowledges the Simons Foun-

dation for financial support (Grant No. 534160). The authors are grateful for providing computational resources of the K computer in RIKEN R-CCS through the HPCI System Research Project (Projects No. hp140130, No. hp150140, No. hp170324, and No. hp180098). The calculations were also performed in part on the RIKEN supercomputer system (HOKUSAI GreatWave) at the Advanced Center for Computing and Communications (ACCC), RIKEN.

[1] Y. Tokura, *J. Phys. Soc. Jpn.* **75**, 011001 (2006).

[2] S. Iwai and H. Okamoto, *J. Phys. Soc. Jpn.* **75**, 011007 (2006).

[3] K. Yonemitsu and K. Nasu, *Phys. Rep.* **465**, 1 (2008).

[4] H. Aoki, N. Tsuji, M. Eckstein, M. Kollar, T. Oka, and P. Werner, *Rev. Mod. Phys.* **86**, 779 (2014).

[5] C. Giannetti, M. Capone, D. Fausti, M. Fabrizio, F. Parmigiani, and D. Mihailovic, *Adv. Phys.* **65**, 58 (2016).

[6] D. Fausti, R. I. Tobey, N. Dean, S. Kaiser, A. Dienst, M. C. Hoffmann, S. Pyon, T. Takayama, H. Takagi, and A. Cavalleri, *Science* **331**, 189 (2011).

[7] W. Hu, S. Kaiser, D. Nicoletti, C. R. Hunt, I. Gierz, M. C. Hoffmann, M. Le Tacon, T. Loew, B. Keimer, and A. Cavalleri, *Nat. Mater.* **13**, 705 (2014).

[8] S. Kaiser, C. R. Hunt, D. Nicoletti, W. Hu, I. Gierz, H. Y. Liu, M. Le Tacon, T. Loew, D. Haug, B. Keimer, and A. Cavalleri, *Phys. Rev. B* **89**, 184516 (2014).

[9] M. Mitrano, A. Cantaluppi, D. Nicoletti, S. Kaiser, A. Perucchi, S. Lupi, P. Di Pietro, D. Pontiroli, M. Riccò, S. R. Clark, D. Jaksch, and A. Cavalleri, *Nature (London)* **530**, 461 (2016).

[10] A. Cantaluppi, M. Buzzi, G. Jotzu, D. Nicoletti, M. Mitrano, D. Pontiroli, M. Riccò, A. Perucchi, P. Di Pietro, and A. Cavalleri, *Nat. Phys.* **14**, 837 (2018).

[11] M. A. Sentef, A. F. Kemper, A. Georges, and C. Kollath, *Phys. Rev. B* **93**, 144506 (2016).

[12] D. M. Kennes, E. Y. Wilner, D. R. Reichman, and A. J. Millis, *Nat. Phys.* **13**, 479 (2017).

[13] K. Ido, T. Ohgoe, and M. Imada, *Sci. Adv.* **3**, e1700718 (2017).

[14] G. Mazza and A. Georges, *Phys. Rev. B* **96**, 064515 (2017).

[15] S. Iwai, M. Ono, A. Maeda, H. Matsuzaki, H. Kishida, H. Okamoto, and Y. Tokura, *Phys. Rev. Lett.* **91**, 057401 (2003).

[16] H. Okamoto, H. Matsuzaki, T. Wakabayashi, Y. Takahashi, and T. Hasegawa, *Phys. Rev. Lett.* **98**, 037401 (2007).

[17] H. Uemura, H. Matsuzaki, Y. Takahashi, T. Hasegawa, and H. Okamoto, *J. Phys. Soc. Jpn.* **77**, 113714 (2008).

[18] H. Okamoto, T. Miyagoe, K. Kobayashi, H. Uemura, H. Nishioka, H. Matsuzaki, A. Sawa, and Y. Tokura, *Phys. Rev. B* **82**, 060513 (2010).

[19] H. Okamoto, T. Miyagoe, K. Kobayashi, H. Uemura, H. Nishioka, H. Matsuzaki, A. Sawa, and Y. Tokura, *Phys. Rev. B* **83**, 125102 (2011).

[20] T. Oka and H. Aoki, *Phys. Rev. B* **78**, 241104 (2008).

[21] T. Oka, *Phys. Rev. B* **86**, 075148 (2012).

[22] M. Eckstein and P. Werner, *Phys. Rev. Lett.* **110**, 126401 (2013).

[23] A. Rosch, D. Rasch, B. Binz, and M. Vojta, *Phys. Rev. Lett.* **101**, 265301 (2008).

[24] J.-S. Bernier, P. Barmettler, D. Poletti, and C. Kollath, *Phys. Rev. A* **87**, 063608 (2013).

[25] S. Kitamura and H. Aoki, *Phys. Rev. B* **94**, 174503 (2016).

[26] See Supplemental Material for details, which includes Refs. [27–35].

[27] T. J. Park and J. Light, *J. Chem. Phys.* **85**, 5870 (1986).

[28] N. Mohankumar and S. M. Auerbach, *Comput. Phys. Commun.* **175**, 473 (2006).

[29] D. Pérez-García, F. Verstraete, M. M. Wolf, and J. I. Cirac, *Quantum Inf. Comput.* **7**, 401 (2007).

[30] S. R. White, *Phys. Rev. Lett.* **69**, 2863 (1992).

[31] U. Schollwöck, *Ann. Phys. (Amsterdam)* **326**, 96 (2011).

[32] M. P. Zaletel, R. S. K. Mong, C. Karrasch, J. E. Moore, and F. Pollmann, *Phys. Rev. B* **91**, 165112 (2015).

[33] <http://itensor.org>.

[34] A. G. Rojo, J. O. Sofo, and C. A. Balseiro, *Phys. Rev. B* **42**, 10241 (1990).

[35] J. Mentink, K. Balzer, and M. Eckstein, *Nat. Commun.* **6**, 6708 (2015).

[36] R. Peierls, *Z. Phys.* **80**, 763 (1933).

[37] A. Takahashi, H. Itoh, and M. Aihara, *Phys. Rev. B* **77**, 205105 (2008).

[38] G. De Filippis, V. Cataudella, E. A. Nowadnick, T. P. Devereaux, A. S. Mishchenko, and N. Nagaosa, *Phys. Rev. Lett.* **109**, 176402 (2012).

[39] H. Lu, S. Sota, H. Matsueda, J. Bonča, and T. Tohyama, *Phys. Rev. Lett.* **109**, 197401 (2012).

[40] H. Hashimoto and S. Ishihara, *Phys. Rev. B* **93**, 165133 (2016).

[41] Y. Wang, M. Claassen, B. Moritz, and T. P. Devereaux, *Phys. Rev. B* **96**, 235142 (2017).

[42] M. Eckstein and P. Werner, *Phys. Rev. B* **84**, 035122 (2011).

[43] P. Werner, K. Held, and M. Eckstein, *Phys. Rev. B* **90**, 235102 (2014).

[44] H. Yanagiya, Y. Tanaka, and K. Yonemitsu, *J. Phys. Soc. Jpn.* **84**, 094705 (2015).

[45] C. N. Yang, *Phys. Rev. Lett.* **63**, 2144 (1989).

[46] F. H. L. Essler, V. E. Korepin, and K. Schoutens, *Phys. Rev. Lett.* **67**, 3848 (1991).

[47] F. H. Essler, V. E. Korepin, and K. Schoutens, *Nucl. Phys. B* **372**, 559 (1992).

[48] F. H. Essler, H. Frahm, F. Göhmann, A. Klümper, and V. E. Korepin, *The One-Dimensional Hubbard Model* (Cambridge University Press, Cambridge, England, 2005).

- [49] $\mathcal{C}_{N_\eta} = N_\eta! \prod_{l=1}^{N_\eta} (L - 2N_0 - l + 1)$ [50].
- [50] M. Takahashi, *Thermodynamics of One Dimensional Solvable Models* (Cambridge University Press, Cambridge, England, 1999).
- [51] Note that $|\psi_{N_\eta}\rangle$ is the exact eigenstate of $\hat{\mathcal{H}}$ with the eigenenergy $E_{N_0} + N_\eta U$, where E_{N_0} is the eigenenergy of $|\psi_{N_0, N_0}^{(\text{GS})}\rangle$.
- [52] J. J. Sakurai, *Modern Quantum Mechanics* (Addison-Wesley, Reading, MA, 1994); M. E. Rose, *Elementary Theory of Angular Momentum* (Wiley, New York, 1967).
- [53] A. Masurenko, C. S. Chiu, G. Ji, M. F. Parsons, M. Kanasz-Nagy, R. Schmidt, F. Grusdt, E. Demler, D. Greif, and M. Greiner, [Nature \(London\) 545, 462 \(2017\)](#)

SUPPLEMENTAL MATERIAL

1. Exact diagonalization method

To evaluate the state $|\Psi(t)\rangle$ under the time-dependent Hamiltonian $\hat{\mathcal{H}}(t)$, we numerically solve the time-dependent Schrödinger equation,

$$i \frac{\partial}{\partial t} |\Psi(t)\rangle = \hat{\mathcal{H}}(t) |\Psi(t)\rangle, \quad (\text{S1})$$

with the initial condition that $|\Psi(t=0)\rangle = |\psi_0\rangle$, where $|\psi_0\rangle$ is the ground state of the Hamiltonian $\hat{\mathcal{H}}(t=0)$. For this purpose, we employ the time-dependent exact diagonalization (ED) method based on the Lanczos algorithm [S1, S2]. In this method, the time evolution with a short time step δt is calculated as

$$\begin{aligned} |\Psi(t+\delta t)\rangle &\simeq e^{-i\hat{\mathcal{H}}(t)\delta t} |\Psi(t)\rangle \\ &\simeq \sum_{\ell=1}^{M_L} e^{-i\xi_\ell \delta t} |\tilde{\psi}_\ell\rangle \langle \tilde{\psi}_\ell | \Psi(t) \rangle, \end{aligned} \quad (\text{S2})$$

where ξ_ℓ and $|\tilde{\psi}_\ell\rangle$ are eigenenergies and eigenvectors of $\hat{\mathcal{H}}(t)$, respectively, in the corresponding Krylov subspace generated with M_L Lanczos iterations [S1–S3]. In our ED calculations, we adopt $\delta t = 0.01/t_h$ and $M_L = 15$ for the time evolution, which provides results with almost machine precision accuracy.

2. One-dimensional (1D) Hubbard model with larger L : a MPS study

Method

In order to confirm the enhancement of the pair correlation in larger systems, we also perform the time-dependent matrix-product state (MPS) [S4] simulation for the time evolution starting from the ground state of the Hubbard model $\hat{\mathcal{H}}$ calculated by the density-matrix renormalization group method [S5, S6]. For the time evolution simulation, we employ the method proposed in Ref. [S7], in which the time evolution operator is factorized as a compact form of the matrix product operator (MPO) representation. In this method, the higher order approximation for the time evolution operator with time step δt are formulated by introducing the additional set of time steps $\{\delta t_1, \delta t_2, \dots, \delta t_n\}$ with complex numbers in order to eliminate the unnecessary lowest order terms arisen from the MPO factorization. The resulting error is $\mathcal{O}(L\delta t^p)$, where L and p denote the system size and the order of the approximation, respectively. Our calculation sets $p = 3$, which requires the additional $n = 4$ time steps, i.e., $\delta t_1 = a+ib$, $\delta t_2 = a-ib$, $\delta t_3 = b+ia$, and $\delta t_4 = b-ia$, with $a = (3 + \sqrt{3})/12$ and $b = (3 - \sqrt{3})/12$.

For the MPS simulation, we use the ITensor package [S8]. We keep the bond dimension up to $m = 1200$ to

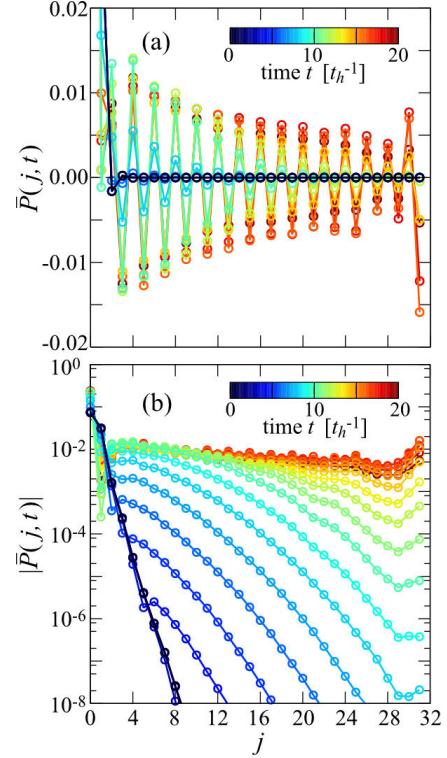


Figure S.1. Time dependence of the on-site pair correlation function (a) $\bar{P}(j, t)$ and (b) logarithm of $|\bar{P}(j, t)|$ calculated by the time-dependent MPS method for a chain of $L = 32$ sites with OBC at $U = 8t_h$. Here, $A_0 = 0.2$, $\omega_p = 8.26t_h$, $\sigma_p = 2/t_h$, and $t_0 = 8/t_h$ are adopted in the vector potential $A(t)$.

calculate the ground state of $\hat{\mathcal{H}}$ for the initial state and $m = 4800$ for the time evolution of the $L = 32$ system under open boundary conditions (OBC). The time step δt is set to be $\delta t = 0.01/t_h$.

Results

Figure S.1 shows the real-space on-site pair correlation function

$$\bar{P}(j, t) = \frac{1}{N_b} \sum_{i=1}^{N_b} \langle \Psi(t) | (\hat{\Delta}_{i+j}^\dagger \hat{\Delta}_i + \text{H.c.}) | \Psi(t) \rangle, \quad (\text{S3})$$

where $\hat{\Delta}_i = \hat{c}_{i,\uparrow} \hat{c}_{i,\downarrow}$ and $N_b = L - j$ is the number of pairs of sites separated by distance j in the system of L sites with OBC. As shown in Fig. S.1, the pair correlation extends to a longer distance gradually with time in the transient period and shows clearly the sign-alternating feature that is characteristic of the η -pairing. The pair correlation eventually reaches to the longest distance in the system, similar to the results shown in Figs. 1(a) and 1(b) in the main text.

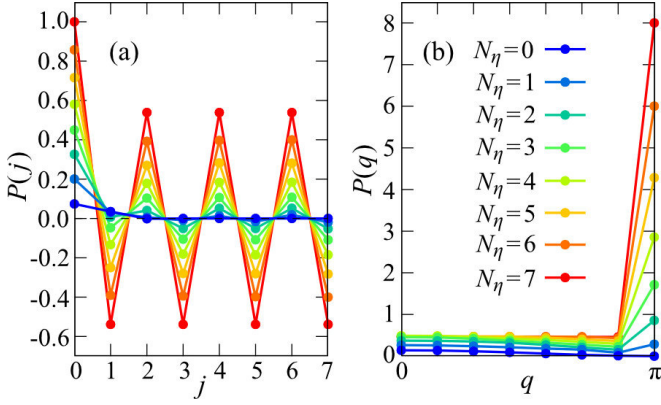


Figure S.2. (a) On-site pair correlation function $P(j)$ and (b) on-site pair structure factor $P(q)$ for the half-filled η -pairing eigenstate $|\psi_{N_\eta}\rangle$ at $U = 8t_h$ with the different number of η pairs N_η ($\leq L/2$). $|\psi_{N_\eta}\rangle$ is generated from the ground state $|\psi_{N_0, N_0}^{(\text{GS})}\rangle$ of the Hubbard model $\hat{\mathcal{H}}$ with $N_0 = L/2 - N_\eta$ calculated by the ED method for $L = 14$ under PBC.

3. η -pairing in the 1D Hubbard model for $L = 14$

As an example, Fig. 3 in the main text shows the on-site pair correlation $P(j)$ and $P(q)$ of the η -pairing eigenstate

$$|\psi_{N_\eta}\rangle = \frac{1}{\sqrt{C_{N_\eta}}} (\hat{\eta}^+)^{N_\eta} |\psi_{N_0, N_0}^{(\text{GS})}\rangle \quad (\text{S4})$$

for $L = 10$ simply because of the correspondence to Fig. 4(a) calculated for the 10 site cluster. Here, we show supplementarily the results of $P(j)$ and $P(q)$ for $L = 14$ at half-filling in Fig. S.2. The ground state $|\psi_{N_0, N_0}^{(\text{GS})}\rangle$ of the Hubbard model $\hat{\mathcal{H}}$ with $N_\uparrow = N_\downarrow = N_0 = L/2 - N_\eta$ is calculated by the ED method under periodic boundary conditions (PBC). Note that $|\psi_{N_\eta}\rangle$ is the eigenstate of $\hat{\mathcal{H}}$ at half-filling with N_η η pairs. As shown in Fig. S.2, the density-wave-like pair correlation is largest for $N_\eta = L/2$.

4. Hubbard model on the square lattice

In the main text, we focus on the 1D Hubbard model to demonstrate that the strong superconducting correlation can be induced in the Mott insulator (MI) by the pulse irradiation, and show that the origin of this superconductivity is due to the η -pairing mechanism. Here, we show that exactly the same conclusion can be reached for the two-dimensional (2D) Hubbard model on the square lattice with only nearest neighbor hoppings.

Model and η operators

The 2D Hubbard model is described by the following Hamiltonian:

$$\hat{\mathcal{H}} = -t_h \sum_{\langle i,j \rangle} \sum_{\sigma} \left(\hat{c}_{i,\sigma}^\dagger \hat{c}_{j,\sigma} + \text{H.c.} \right) + U \sum_i \hat{n}_{i,\uparrow} \hat{n}_{i,\downarrow}, \quad (\text{S5})$$

where the sum $\langle i,j \rangle$ runs over all pairs of nearest neighbor sites i and j on the square lattice. Similarly to the 1D case, the total $\hat{\eta}$ operators $\hat{\eta}^\pm = \sum_j \hat{\eta}_j^\pm$ and $\hat{\eta}_z = \sum_j \hat{\eta}_j^z$ are defined in terms of the local operators $\hat{\eta}_j^+ = (-1)^{j_x+j_y} \hat{c}_{j,\downarrow}^\dagger \hat{c}_{j,\uparrow}^\dagger$, $\hat{\eta}_j^- = (-1)^{j_x+j_y} \hat{c}_{j,\uparrow} \hat{c}_{j,\downarrow}$, and $\hat{\eta}_j^z = \frac{1}{2} (\hat{n}_{j,\uparrow} + \hat{n}_{j,\downarrow} - 1)$, where the location of site j is given as $\mathbf{R}_j = j_x \mathbf{e}_x + j_y \mathbf{e}_y$ and $\mathbf{e}_{x(y)}$ is the unit vector along the $x(y)$ direction. These operators satisfy the $SU(2)$ commutation relations. We can also show that $[\hat{\mathcal{H}}, \hat{\eta}^\pm] = \pm U \hat{\eta}^\pm$ and $[\hat{\mathcal{H}}, \hat{\eta}^+ \hat{\eta}^-] = [\hat{\mathcal{H}}, \hat{\eta}_z] = 0$. Therefore, any eigenstate of the Hubbard model $\hat{\mathcal{H}}$ can be chosen also to be an eigenstate $|\eta, \eta_z\rangle$ of $\hat{\eta}^2 = \frac{1}{2} (\hat{\eta}^+ \hat{\eta}^- + \hat{\eta}^- \hat{\eta}^+) + \hat{\eta}_z^2$ and $\hat{\eta}_z$ with the eigenvalues $\eta(\eta+1)$ and η_z , respectively, where $|\eta, \eta_z\rangle$ can take $\eta = 0, 1, 2, \dots, L/2$ and $\eta_z = -\eta, -\eta+1, \dots, \eta$, assuming that the number N_\uparrow of up electrons and the number N_\downarrow of down electrons are the same and L (even) is the total number of sites. At half-filling with $N_\uparrow = N_\downarrow = L/2$, the eigenstates are characterized with $\eta = 0, 1, 2, \dots, L/2$ and $\eta_z = 0$, and the ground state $|\psi_0\rangle$ of the Hubbard model $\hat{\mathcal{H}}$ is $\eta = \eta_z = 0$.

The real-space on-site pair correlation function for the time-evolved state $|\Psi(t)\rangle$ is defined as

$$P(\mathbf{R}_j, t) = \frac{1}{L} \sum_i \langle \Psi(t) | \left(\hat{\Delta}_{\mathbf{R}_i + \mathbf{R}_j}^\dagger \hat{\Delta}_{\mathbf{R}_i} + \text{H.c.} \right) | \Psi(t) \rangle, \quad (\text{S6})$$

where $\hat{\Delta}_{\mathbf{R}_i} = \hat{c}_{i,\uparrow}^\dagger \hat{c}_{i,\downarrow}$ and the pair structure factor in the momentum space is given as

$$P(\mathbf{q}, t) = \sum_j e^{i\mathbf{q} \cdot \mathbf{R}_j} P(\mathbf{R}_j, t). \quad (\text{S7})$$

Noticing that $\hat{\Delta}_{\mathbf{R}_j} = (-1)^{j_x+j_y} \hat{\eta}_j^-$, $P(\mathbf{q}, t)$ at $\mathbf{q} = \mathbf{\pi} = (\pi, \pi)$ is

$$P(\mathbf{q} = \mathbf{\pi}, t) = \frac{2}{L} \langle \Psi(t) | \hat{\eta}^+ \hat{\eta}^- | \Psi(t) \rangle \quad (\text{S8})$$

$$= \frac{2}{L} \langle \Psi(t) | (\hat{\eta}^2 - \hat{\eta}_z^2 + \hat{\eta}_z) | \Psi(t) \rangle. \quad (\text{S9})$$

The pair structure factor $P(\mathbf{q} = \mathbf{\pi})$ for $|\eta, \eta_z\rangle$ is thus $2[\eta(\eta+1) - \eta_z(\eta_z-1)]/L$.

Any eigenstate $|\eta, \eta_z\rangle$ can be constructed from the LWS $|\eta, -\eta\rangle$ by repeatedly applying $\hat{\eta}^+$ because

$$\hat{\eta}^+ |\eta, \eta_z\rangle = \sqrt{\eta(\eta+1) - \eta_z(\eta_z+1)} |\eta, \eta_z+1\rangle. \quad (\text{S10})$$

Since $\hat{\eta}^- |\eta, -\eta\rangle = 0$ by definition, the LWS contains no η pairs and $P(\mathbf{q} = \mathbf{\pi}) = 0$. Each time that $\hat{\eta}^+$ is applied from the LWS, the number of η pairs increases by

one, and the maximum number of η pairs is obtained when $\eta_z = 0$ (i.e., half-filling) for a given η , where $\langle \eta, \eta_z = 0 | \hat{\eta}^+ \hat{\eta}^- | \eta, \eta_z = 0 \rangle = \eta(\eta + 1)$ and the number of η pairs is η .

The time-dependent external field is introduced in Eq. (S5) by $t_h \hat{c}_{i,\sigma}^\dagger \hat{c}_{j,\sigma} \rightarrow t_h e^{-i\mathbf{A}(t) \cdot (\mathbf{R}_i - \mathbf{R}_j)} \hat{c}_{i,\sigma}^\dagger \hat{c}_{j,\sigma}$ with the time-dependent vector potential $\mathbf{A}(t) = A(t)(\mathbf{e}_x + \mathbf{e}_y)$ pointing along the diagonal direction and $A(t)$ given in the main text. The current operator $\hat{J}_\alpha^{(0)}$ along a direction α ($\alpha = x, y$) is defined as

$$\hat{J}_\alpha^{(0)} = it_h \sum_{j,\sigma} \left(\hat{c}_{j+\mathbf{e}_\alpha,\sigma}^\dagger \hat{c}_{j,\sigma} - \hat{c}_{j,\sigma}^\dagger \hat{c}_{j+\mathbf{e}_\alpha,\sigma} \right), \quad (\text{S11})$$

where $\hat{c}_{j+\mathbf{e}_\alpha,\sigma}^\dagger$ is the creation operator of an electron at the site located at $\mathbf{R}_j + \mathbf{e}_\alpha$ with spin σ . We can now show that

$$[\hat{\eta}^\pm, \hat{J}_\alpha^{(0)}] = \sqrt{2} \hat{J}_\alpha^{(\pm 1)}, \quad [\hat{\eta}_z, \hat{J}_\alpha^{(0)}] = 0, \quad (\text{S12})$$

$$[\hat{\eta}^\pm, \hat{J}_\alpha^{(\mp 1)}] = \sqrt{2} \hat{J}_\alpha^{(0)}, \quad [\hat{\eta}_z, \hat{J}_\alpha^{(\pm 1)}] = \pm \hat{J}_\alpha^{(\pm 1)}, \quad (\text{S13})$$

where

$$\hat{J}_\alpha^{(+1)} = \sqrt{2} it_h \sum_j (-1)^{j_x + j_y} (\hat{c}_{j+\mathbf{e}_\alpha,\uparrow}^\dagger \hat{c}_{j,\downarrow}^\dagger + \hat{c}_{j,\uparrow}^\dagger \hat{c}_{j+\mathbf{e}_\alpha,\downarrow}^\dagger), \quad (\text{S14})$$

and

$$\hat{J}_\alpha^{(-1)} = \sqrt{2} it_h \sum_j (-1)^{j_x + j_y} (\hat{c}_{j+\mathbf{e}_\alpha,\downarrow}^\dagger \hat{c}_{j,\uparrow}^\dagger + \hat{c}_{j,\downarrow}^\dagger \hat{c}_{j+\mathbf{e}_\alpha,\uparrow}^\dagger). \quad (\text{S15})$$

Therefore, $\hat{J}_\alpha^{(q)}$ with $q = 0, \pm 1$ is a rank-one tensor operator in terms of $\hat{\eta}$ operators. In particular, the current operator $\hat{J}_\alpha^{(0)}$ is a rank-one tensor operator with $q = 0$ and hence there is the following selection rule: $\langle \eta', \eta'_z | \hat{J}_\alpha^{(0)} | \eta, \eta_z \rangle \neq 0$ only for $\eta' = \eta \pm 1$ when $\eta'_z = \eta_z = 0$ [S9, S10]. We also note that $it_h \sum_{\langle i,j \rangle} \sum_\sigma \sin [\mathbf{A}(t) \cdot (\mathbf{R}_i - \mathbf{R}_j)] (\hat{c}_{i,\sigma}^\dagger \hat{c}_{j,\sigma} - \text{H.c.})$ is a rank-one tensor operator with $q = 0$, while $-t_h \sum_{\langle i,j \rangle} \sum_\sigma \cos [\mathbf{A}(t) \cdot (\mathbf{R}_i - \mathbf{R}_j)] (\hat{c}_{i,\sigma}^\dagger \hat{c}_{j,\sigma} + \text{H.c.})$ is a rank-zero tensor operator, i.e., a scalar operator.

Although here we consider the 2D case, the extension to other spatial dimensions is straightforward.

Results

As shown above, any eigenstate of $\hat{\mathcal{H}}$ can be chosen to be an eigenstate of $\hat{\eta}^2$ and $\hat{\eta}_z$. Figure S.3(a) shows all the eigenenergies ε_m of $\hat{\mathcal{H}}$ and the corresponding pair structure factors $P(\mathbf{q})$ at $\mathbf{q} = \mathbf{\pi} = (\pi, \pi)$ on a $\sqrt{10} \times \sqrt{10}$ cluster with PBC at half-filling. Indeed, as in the 1D case, $P(\mathbf{\pi})$ is quantized as $P(\mathbf{\pi}) = 2\eta(\eta + 1)/L$, where $\eta (= 0, 1, \dots, L/2)$ corresponds to the number of η pairs.

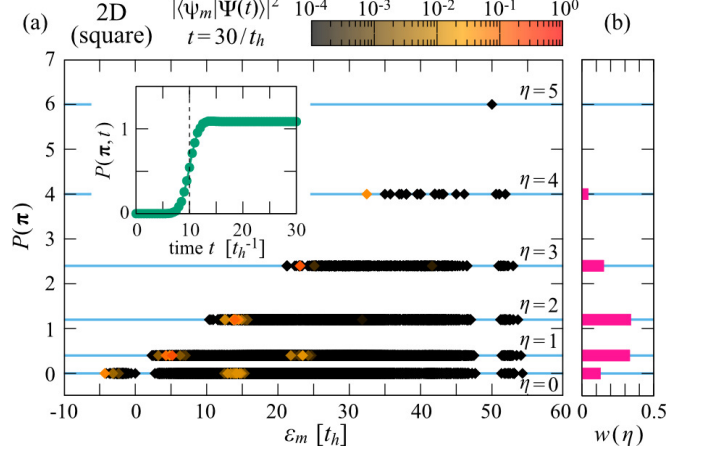


Figure S.3. (a) All eigenenergies ε_m and $P(\mathbf{q} = \mathbf{\pi})$ [$\mathbf{\pi} = (\pi, \pi)$] for the eigenstates $|\psi_m\rangle$ of the half-filled Hubbard model on a $\sqrt{10} \times \sqrt{10}$ cluster with PBC at $U = 10t_h$. The color of each point (diamond) indicates the weight $|\langle \psi_m | \Psi(t) \rangle|^2$ of the eigenstate $|\psi_m\rangle$ in the photoinduced state $|\Psi(t)\rangle$ at $t = 30/t_h$. Here, $A_0 = 0.25$, $\omega_p = 9.1t_h$, $\sigma_p = 2/t_h$, and $t_0 = 10/t_h$ are adopted in the vector potential $A(t)$. When the eigenstates are degenerate, the color indicates the sum of $|\langle \psi_m | \Psi(t) \rangle|^2$ over these degenerate states. The time evolution of $P(\mathbf{q} = \mathbf{\pi}, t)$ for $|\Psi(t)\rangle$ is also shown in the inset. (b) The total weight $w(\eta)$ of $|\langle \psi_m | \Psi(t) \rangle|^2$ over the states $|\psi_m\rangle$ that have the same number η of η pairs, and thus $\sum_{\eta=0}^{L/2} w(\eta) = 1$. The parameters are the same as in (a).

As shown in Fig S.3(b), the photoinduced state $|\Psi(t)\rangle$ after the pulse irradiation displays nonzero overlaps with the eigenstates $|\psi_m\rangle$ of $\hat{\mathcal{H}}$ with $\eta \neq 0$. This is responsible for the large enhancement of $P(\mathbf{q}, t)$ in the photoinduced state $|\Psi(t)\rangle$ [see the inset of Fig. S.3(a)]. Since the current operator is a rank-one tensor operator, we can again observe in Fig. S.3(a) a “tower of states” structure of the eigenstates $|\psi_m\rangle$ contributing to the photoinduced state $|\Psi(t)\rangle$ with large weights $|\langle \psi_m | \Psi(t) \rangle|^2$.

5. 1D Hubbard model away from half-filling

We also examine the behavior of the photoinduced states in the 1D Hubbard model $\hat{\mathcal{H}}$ away from half-filling. Figure S.4 shows the time evolution of the pair correlation function $P(j, t)$ calculated by the ED method for $L = 12$ with $N_\uparrow = N_\downarrow = 5$ (10 electrons in total) under PBC. Although the magnitude of $P(j, t)$ is smaller than that for the case of half-filling, $P(j, t)$ clearly shows a pair density wave like oscillation with the correlation extended up to the longest distance of the cluster. Therefore, the η -pairing correlation is induced in the photoexcited state in the Hubbard model even away from half-filling.

To elucidate the nature of the photoinduced state $|\Psi(t)\rangle$ in terms of the η pairs, we calculate the eigenen-

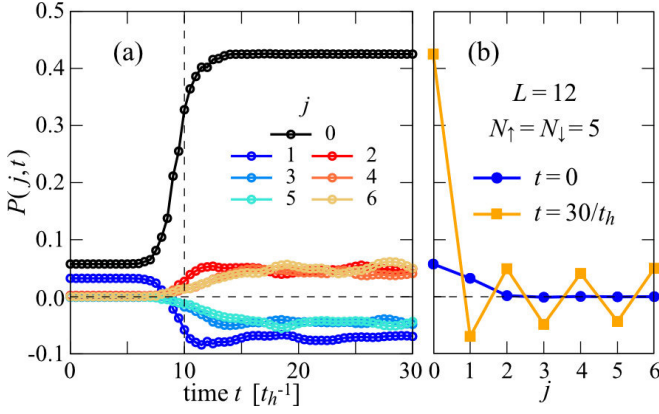


Figure S.4. (a) Time evolution of the on-site pair correlation function $P(j,t)$ with hole doping. (b) $P(j,t)$ at $t = 0$ (blue circles) and $t = 30/t_h$ (orange squares). The results are calculated by the ED method for $L = 12$ and $N_\uparrow = N_\downarrow = 5$ at $U = 8t_h$ with $\sigma_p = 2/t_h$, $t_0 = 10/t_h$, $A_0 = 0.7$, and $\omega_p = 8.8t_h$.

ergies ε_m and the structure factors $P(q = \pi)$ for all the eigenstates $|\psi_m\rangle$ of the 1D Hubbard model $\hat{\mathcal{H}}$ with hole-doping. Figure S.5 shows the results for $L = 8$ with $N_\uparrow = N_\downarrow = 3$ (6 electrons in total) under PBC. As shown in Fig. S.5(a), the structure factor $P(q = \pi)$ for each eigenstate is nicely quantized. This is because each eigenstate $|\psi_m\rangle$ away from half-filling is also the eigenstate of $\hat{\eta}^2$ and $\hat{\eta}_z$. The quantized values are given as

$$P(q=\pi) = \frac{2}{L} \langle \psi_m | \hat{\eta}^+ \hat{\eta}^- | \psi_m \rangle = \frac{2}{L} \langle \psi_m | (\hat{\eta}^2 - \hat{\eta}_z^2 + \hat{\eta}_z) | \psi_m \rangle = \frac{2}{L} [\eta(\eta+1) - \eta_z(\eta_z-1)] \quad (\text{S16})$$

with $\eta = |\eta_z|$, $|\eta_z|+1, \dots, \frac{L}{2}$ and $\eta_z = (N_\uparrow + N_\downarrow - L)/2 = -1$. Note that $P(\pi) = 0$ (no η pair state) is characterized by the state with $\eta = 1$ because $\eta_z = -1$ and this state is the LWS.

In Fig. S.5(a), the color of each point indicates the weight $|\langle \psi_m | \Psi(t) \rangle|^2$ of the eigenstate $|\psi_m\rangle$ in the photoinduced state $|\Psi(t)\rangle$ that exhibits the enhancement of $P(q = \pi, t)$ after the pulse irradiation [see the inset of Fig S.5(a)]. We find that the state $|\Psi(t)\rangle$ after the pulse irradiation contains the nonzero weights of the eigenstates $|\psi_m\rangle$ with finite $P(\pi)$ [also see Fig. S.5(b)]. Therefore, the reason for the enhancement of $P(q = \pi, t)$ is the same as in the case at half-filling.

However, the distribution of the weight $|\langle \psi_m | \Psi(t) \rangle|^2$ after the pulse irradiation in Fig. S.5(a) is qualitatively different from that in the case at half-filling shown in Fig. 4(a) in the main text. For example, there is the finite contribution to the weight from the eigenstates with $P(\pi) = 0$ around $\varepsilon_m - \varepsilon_0 \sim \omega_p$, which is absent at half-filling. This is explained by the different selection rules of the current operator \hat{J} for the half-filled ($\eta_z = 0$) and hole-doped ($\eta_z \neq 0$) states. As mentioned in the main text and also in Sec. 4, \hat{J} is a rank-one tensor operator

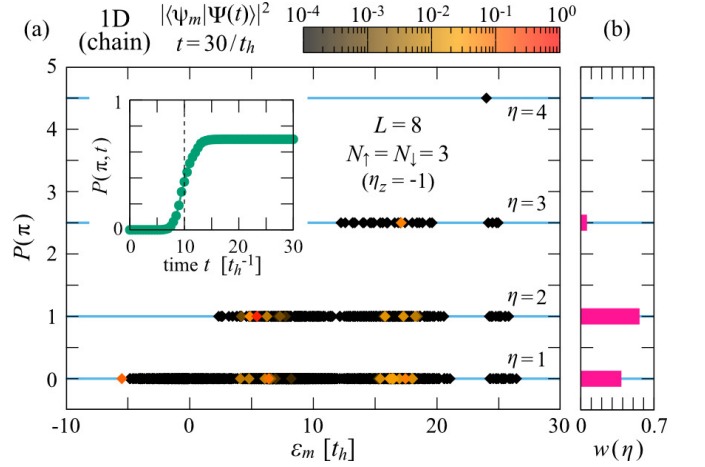


Figure S.5. (a) All eigenenergies ε_m and $P(q = \pi)$ for the eigenstates $|\psi_m\rangle$ of the hole-doped 1D Hubbard model $\hat{\mathcal{H}}$ at $U = 8t_h$ for $L = 8$ under PBC with $N_\uparrow = N_\downarrow = 3$ electrons. The color of each point (diamond) indicates the weight $|\langle \psi_m | \Psi(t) \rangle|^2$ of the eigenstate $|\psi_m\rangle$ in the photoinduced state $|\Psi(t)\rangle$ at $t = 30/t_h$. Here, $A_0 = 0.7$, $\omega_p = 10.7t_h$, $\sigma_p = 2/t_h$, and $t_0 = 10/t_h$ are adopted in the vector potential $A(t)$. When the eigenstates are degenerate, the color indicates the sum of $|\langle \psi_m | \Psi(t) \rangle|^2$ over these degenerate states. The time evolution of $P(q = \pi, t)$ for $|\Psi(t)\rangle$ is also shown in the inset. (b) The total weight $w(\eta)$ of $|\langle \psi_m | \Psi(t) \rangle|^2$ over the states $|\psi_m\rangle$ that have the same eigenvalue of η , and thus $\sum_{\eta} w(\eta) = 1$. The parameters are the same as in (a). Note that the number of η pairs is $\eta - 1$ for this hole-doped case.

with the zeroth component in terms of the $\hat{\eta}$ operators. Hence, from the Wigner–Eckart theorem [S9, S10], the selection rule of $\langle \eta', \eta_z | \hat{J} | \eta, \eta_z \rangle$ is given as

$$\langle \eta', \eta'_z | \hat{J} | \eta, \eta_z \rangle \propto \begin{pmatrix} \eta & 1 & \eta' \\ \eta_z & 0 & -\eta'_z \end{pmatrix} \quad (\text{S17})$$

with the $3j$ -symbol. The $3j$ -symbol is zero unless $\eta - 1 \leq \eta' \leq \eta + 1$ and $\eta_z - \eta'_z = 0$ are satisfied. Therefore, $\langle \eta', \eta'_z | \hat{J} | \eta, \eta_z \rangle \neq 0$ for $\eta' = \eta$, $\eta \pm 1$ when $\eta'_z = \eta_z \neq 0$ for the hole-doped states. The result in Fig. S.5(a) follows this selection rule. However, when $\eta_z = \eta'_z = 0$ for the half-filled state, the nonzero $3j$ -symbol must satisfy the additional rule: $\eta + \eta' + 1 = (\text{even})$. Therefore, the excitation to the states with $\eta' = \eta$ is not induced by \hat{J} at half-filling ($\eta_z = \eta'_z = 0$), and $\langle \eta', 0 | \hat{J} | \eta, 0 \rangle \neq 0$ only for $\eta' = \eta \pm 1$. The results at half-filling in Fig. 4(a) in the main text and Fig. S.3(a) follow this selection rule.

6. Perturbation analysis in the limit of large pulse width σ_p

In the large pulse width limit, i.e., $\sigma_p \rightarrow \infty$, the time-dependent vector potential is given as $A(t) = A_0 \cos[\omega_p(t - t_0)]$. Let us denote the time-dependent

Hamiltonian with the time-dependent external field as

$$\hat{\mathcal{H}}(t) = \hat{\mathcal{H}} + \hat{\mathcal{V}}(t), \quad (\text{S18})$$

where $\hat{\mathcal{H}}$ is the time-independent part of the Hamiltonian given by, e.g., Eq. (1) in the main text and $\hat{\mathcal{V}}(t)$ is the time-dependent part of the Hamiltonian given as

$$\hat{\mathcal{V}}(t) = -t_h \sum_{j,\sigma} \left(e^{iA(t)} - 1 \right) \hat{c}_{j,\sigma}^\dagger \hat{c}_{j+1,\sigma} + \text{H.c..} \quad (\text{S19})$$

Because $A(t)$ becomes a periodic function of t in the limit $\sigma_p \rightarrow \infty$, $\hat{\mathcal{V}}(t)$ can be expanded using Bessel functions of the first kind $\mathcal{J}_\mu(x)$ (μ : integer) [S11], i.e.,

$$\hat{\mathcal{V}}(t) = \sum_{\mu=-\infty}^{\infty} \hat{\mathcal{V}}^{(\mu)} e^{-i\mu\omega_p t}, \quad (\text{S20})$$

where

$$\begin{aligned} \hat{\mathcal{V}}^{(0)} &= (\mathcal{J}_0(A_0) - 1)\hat{K}, \\ \hat{\mathcal{V}}^{(2\mu)} &= (-1)^\mu \mathcal{J}_{2\mu}(A_0)\hat{K}, \quad (\mu \neq 0) \\ \hat{\mathcal{V}}^{(2\mu+1)} &= (-1)^\mu \mathcal{J}_{2\mu+1}(A_0)\hat{J}. \end{aligned} \quad (\text{S21})$$

Here we set $t_0 = 0$. It is important to notice in Eqs. (S20) and (S21) that the operator \hat{K} in the μ even terms is the

kinetic (rank-zero tensor) operator, i.e.,

$$\hat{K} = -t_h \sum_{j,\sigma} \left(\hat{c}_{j,\sigma}^\dagger \hat{c}_{j+1,\sigma} + \hat{c}_{j+1,\sigma}^\dagger \hat{c}_{j,\sigma} \right), \quad (\text{S22})$$

while the operator \hat{J} in the μ odd terms is the current (rank-one tensor) operator, i.e.,

$$\hat{J} = -it_h \sum_{j,\sigma} \left(\hat{c}_{j,\sigma}^\dagger \hat{c}_{j+1,\sigma} - \hat{c}_{j+1,\sigma}^\dagger \hat{c}_{j,\sigma} \right), \quad (\text{S23})$$

as defined also in the main text.

A time-dependent state $|\Psi(t)\rangle$ governed by $\hat{\mathcal{H}}(t)$ can be expanded as

$$|\Psi(t)\rangle = \sum_m c_m(t) |\psi_m\rangle, \quad (\text{S24})$$

where $|\psi_m\rangle$ ($m = 0, 1, 2, \dots$) are the m th eigenstate of $\hat{\mathcal{H}}$ with the eigenenergy ε_m . For simplicity, we assume that the ground state is not degenerate with $\varepsilon_0 < \varepsilon_1 \leq \varepsilon_2 \leq \dots$. By using the time-dependent perturbation theory, the coefficient $c_m(t)$ is obtained as the sum over terms $c_m^{(k)}(t)$ of the k th order expansion in terms of $\hat{\mathcal{V}}(t)$:

$$c_m(t) = \sum_{k=0}^{\infty} c_m^{(k)}(t). \quad (\text{S25})$$

Assuming that the initial state at time $t_i = -\infty$ is the ground state $|\psi_0\rangle$ of $\hat{\mathcal{H}}$, $c_m^{(k)}(t)$ is given as

$$c_m^{(k)}(t) = (-i)^k \int_{-\infty}^t dt_k \cdots \int_{-\infty}^{t_3} dt_2 \int_{-\infty}^{t_2} dt_1 \sum_{m_{k-1}} \cdots \sum_{m_2} \sum_{m_1} \langle \psi_m | \hat{\mathcal{V}}_I(t_k) | \psi_{m_{k-1}} \rangle \cdots \langle \psi_{m_2} | \hat{\mathcal{V}}_I(t_2) | \psi_{m_1} \rangle \langle \psi_{m_1} | \hat{\mathcal{V}}_I(t_1) | \psi_0 \rangle, \quad (\text{S26})$$

where $\hat{\mathcal{V}}_I(t) = e^{i\hat{\mathcal{H}}t} \hat{\mathcal{V}}(t) e^{-i\hat{\mathcal{H}}t}$ [S9]. Because of Eq. (S20),

$$\langle \psi_m | \hat{\mathcal{V}}_I(t) | \psi_{m'} \rangle = \sum_{\mu} e^{i(\varepsilon_m - \varepsilon_{m'} - \mu\omega_p)t} \mathcal{V}_{mm'}^{(\mu)}, \quad (\text{S27})$$

with

$$\mathcal{V}_{mm'}^{(\mu)} = \langle \psi_m | \hat{\mathcal{V}}^{(\mu)} | \psi_{m'} \rangle. \quad (\text{S28})$$

Therefore, we obtain for $t \rightarrow \infty$ that

$$\begin{aligned} c_m^{(k)}(\infty) &= 2\pi i (-1)^k \sum_{\mu_k} \cdots \sum_{\mu_2} \sum_{\mu_1} \sum_{m_{k-1}} \cdots \sum_{m_2} \sum_{m_1} \mathcal{V}_{mm_{k-1}}^{(\mu_k)} \cdots \mathcal{V}_{m_2 m_1}^{(\mu_2)} \mathcal{V}_{m_1 0}^{(\mu_1)} \prod_{k'=1}^{k-1} \frac{1}{\varepsilon_{m_{k'}} - \varepsilon_0 - \left(\sum_{\ell=1}^{k'} \mu_{\ell} \right) \omega_p - i\gamma} \\ &\times \delta \left(\varepsilon_m - \varepsilon_0 - \left(\sum_{\ell=1}^k \mu_{\ell} \right) \omega_p \right), \end{aligned} \quad (\text{S29})$$

where $\gamma \rightarrow 0^+$ is a convergence factor.

It is now obvious from the delta function in Eq. (S29)

that the coefficients $c_m^{(k)}(t)$ for $t \rightarrow \infty$ can be nonzero only

if $\varepsilon_m - \varepsilon_0 = \left(\sum_{\ell=1}^k \mu_{\ell}\right) \omega_p$, suggesting that the excitations are allowed only to states with the excitation energy that is an integer multiple of ω_p . This nicely explains the energy dependence found in Fig. 4(a) in the main text and Fig. S.3(a) for half-filling and also in Fig. S.5(a) away from half-filling. For example, if $\sum_{\ell} \mu_{\ell} = 2\nu + 1$ (ν : integer), $\mathcal{V}_{mm_{k-1}}^{(\mu_k)} \cdots \mathcal{V}_{m_2 m_1}^{(\mu_2)} \mathcal{V}_{m_1 0}^{(\mu_1)}$ should involve the odd number of excitations induced by the current operator \hat{J} . In the case of half-filling, combining this with the selection rule in Eq. (S17) yields that the η odd excitations are possible if and only if $\varepsilon_m - \varepsilon_0 = (2\nu + 1)\omega_p$. Similarly, the η even excitations are possible if and only if the $\varepsilon_m - \varepsilon_0 = 2\nu\omega_p$ at half-filling. These are in accordance with the “tower of states” structure shown schematically in Fig. 4(c) in the main text.

7. 1D Hubbard model with the next-nearest-neighbor hopping

In this and the next sections, we investigate the pair correlations when the η commutation relations, e.g. $[\hat{\mathcal{H}}, \hat{\eta}^{\pm}] = \pm U \hat{\eta}^{\pm}$, are broken in the Mott-Hubbard system. First, we consider the 1D Hubbard model with the next-nearest-neighbor (NNN) hopping t'_h described by $\hat{\mathcal{H}}_{\text{NNN}} = \hat{\mathcal{H}} + \hat{\mathcal{H}}_{t'_h}$, where $\hat{\mathcal{H}}$ is given by Eq. (1) in the main text and

$$\hat{\mathcal{H}}_{t'_h} = -t'_h \sum_{j,\sigma} (\hat{c}_{j,\sigma}^{\dagger} \hat{c}_{j+2,\sigma} + \text{H.c.}) \quad (\text{S30})$$

is the NNN hopping term. Because $[\hat{\mathcal{H}}_{t'_h}, \hat{\eta}^+] = -4t'_h \sum_k \cos(2k) \hat{c}_{\pi-k,\downarrow}^{\dagger} \hat{c}_{k,\uparrow}^{\dagger} \neq 0$, the Hamiltonian $\hat{\mathcal{H}}_{\text{NNN}}$ breaks the η commutation relations.

Figure S.6 shows the time dependence of the pair correlation functions for the photoexcited state $|\Psi(t)\rangle$ with different values of t'_h calculated by the ED method for $L = 14$ under PBC. As in the main text, the time-dependent external field is introduced via the Peierls phase through the time-dependent vector potential $A(t)$, where the Peierls phase for the NNN hopping t'_h is given as $t'_h \hat{c}_{j,\sigma}^{\dagger} \hat{c}_{j+2,\sigma} \rightarrow t'_h e^{2iA(t)} \hat{c}_{j,\sigma}^{\dagger} \hat{c}_{j+2,\sigma}$ and the form of $A(t)$ is described in the main text.

Although the η commutation relations are broken when t'_h is finite in $\hat{\mathcal{H}}_{\text{NNN}}$, we find the enhancement of the pair correlation functions, specially during the transient period, with the η -pairing like sign-alternating oscillation [see Fig. S.6(b)]. Note that, unlike in the case of $t'_h = 0$, $P(q=\pi, t)$ is no longer conserved after the pulse irradiation because of $[\hat{\mathcal{H}}_{t'_h}, \hat{\eta}^+ \hat{\eta}^-] \neq 0$. With increasing t'_h , $P(j, t)$ at $j > 0$ becomes suppressed and eventually show no longer range correlation after the pulse irradiation [see Fig. S.6(c)]. Therefore, we conclude that the photoinduced states still show the robust η -pairing correlations transiently as long as the NNN hopping t'_h is small, although the large NNN hopping t'_h is unfavorable for the photoinduced η -pairing.

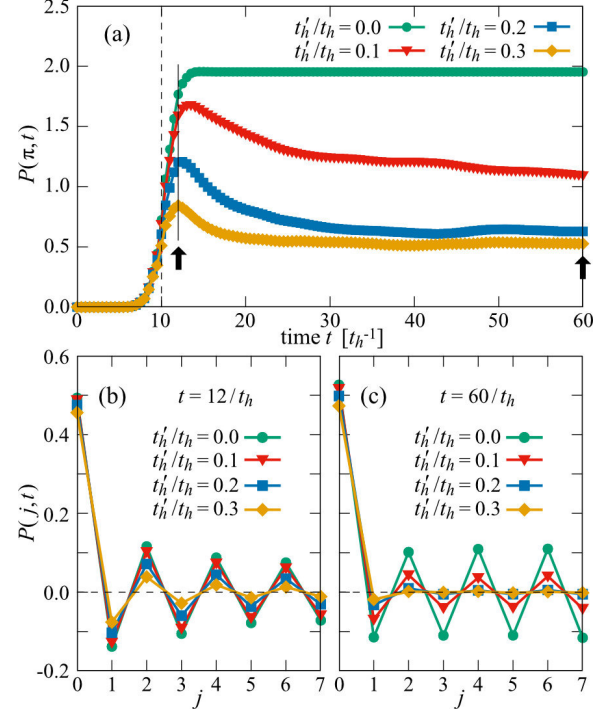


Figure S.6. (a) Time evolution of the pair structure factor $P(q=\pi, t)$ in the 1D Hubbard model with the NNN hopping t'_h at half-filling. Two arrows indicate the time, $t = 12/t_h$ and $60/t_h$, at which the real-space pair correlation function $P(j, t)$ is calculated in (b) and (c), respectively. Note that $t = 12/t_h$ in (b) is within the transient period. The results are calculated by the ED method for $L = 14$ (PBC) at $U = 8t_h$ with $A_0 = 0.4$, $\omega_p = 8.2t_h$, $\sigma_p = 2/t_h$, and $t_0 = 10/t_h$ for the time-dependent vector potential $A(t)$.

8. 1D Hubbard model with the nearest-neighbor Coulomb interaction

In addition, we examine the influence of the nearest-neighbor Coulomb interaction V on the pair correlation in the photoinduced state. The model considered here is the 1D extended Hubbard model described by $\hat{\mathcal{H}}_{\text{EH}} = \hat{\mathcal{H}} + \hat{\mathcal{H}}_V$, where the intersite Coulomb interaction term is given as

$$\hat{\mathcal{H}}_V = V \sum_{j,\sigma,\sigma'} \hat{n}_{j,\sigma} \hat{n}_{j+1,\sigma'}. \quad (\text{S31})$$

Because $[\hat{\mathcal{H}}_V, \hat{\eta}^+] = 2V \sum_{j,\sigma} (-1)^j \hat{c}_{j,\downarrow}^{\dagger} \hat{c}_{j,\uparrow}^{\dagger} (\hat{n}_{j-1,\sigma} + \hat{n}_{j+1,\sigma})$, the Hamiltonian $\hat{\mathcal{H}}_{\text{EH}}$ breaks the η commutation relations. Figure S.7 shows the time dependence of the pair correlation functions for the photoexcited state $|\Psi(t)\rangle$ with different values of V calculated by the ED method for $L = 14$ under PBC. The time-dependent external field is introduced exactly in the same form described in the main text.

Although the η commutation relations are broken when V is finite in $\hat{\mathcal{H}}_{\text{EH}}$, we find the enhancement of

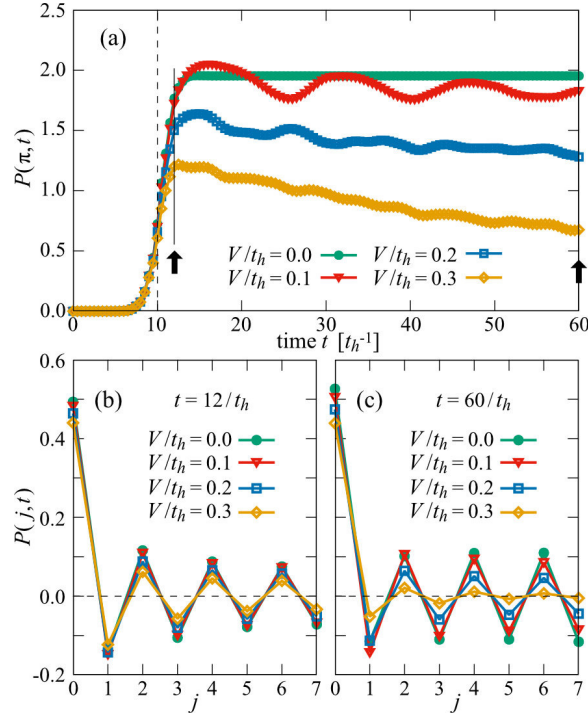


Figure S.7. (a) Time evolution of the pair structure factor $P(q = \pi, t)$ in the 1D Hubbard model with the nearest-neighbor Coulomb interaction V at half-filling. Two arrows indicate the time, $t = 12/t_h$ and $60/t_h$, at which the real-space pair correlation function $P(j, t)$ is calculated in (b) and (c), respectively. Note that $t = 12/t_h$ in (b) is within the transient period. The results are calculated by the ED method for $L = 14$ (PBC) at $U = 8t_h$ with $A_0 = 0.4$, $\omega_p = 8.2t_h$, $\sigma_p = 2/t_h$, and $t_0 = 10/t_h$ for the time-dependent vector potential $A(t)$.

the pair correlation functions at least in the transient period of the pulse irradiation, clearly exhibiting the η -pairing like sign-alternating oscillation [see Fig. S.7(b)]. However, when V is relatively large, the pair correlation is quickly suppressed with increasing t after the pulse irradiation [see Fig. S.7(c)]. Therefore, we conclude that the photoexcited state can still show the robust pair correlation in the transient period, but the strong intersite Coulomb interaction V can eventually disturb the photoinduced η -pairing completely for large t .

9. Other related studies for η -pairing

In nonequilibrium contexts, possible realization of the η -pairing state has also been proposed in the repulsive Hubbard systems with the harmonic trapping potential [S12] and with the dissipative coupling [S13]. However, unlike these studies, our mechanism shown here is based on the selection rule derived from the commutation relation between the η pair and current \hat{J} operators, and therefore provides a completely different pathway of η pair generation.

In the attractive Hubbard model, Kitamura and Aoki have investigated the η -pairing state induced by the periodically driven field [S11]. Based on the Floquet formalism for the effective model in the strong coupling limit, composed of the pair hopping term and the nearest-neighbor pair repulsion, which can be mapped onto a Heisenberg like model [S14], they have shown that the η -pairing state can be induced from the s -wave superconducting state by varying the effective model parameters [S11]. However, the corresponding argument cannot be applied to the repulsive Hubbard model [S15], and thus our mechanism also differs from their suggestion.

[S1] T. J. Park and J. Light, *J. Chem. Phys.* **85**, 5870 (1986).
 [S2] N. Mohankumar and S. M. Auerbach, *Comput. Phys. Commun.* **175**, 473 (2006).
 [S3] H. Hashimoto and S. Ishihara, *Phys. Rev. B* **93**, 165133 (2016).
 [S4] D. Pérez-García, F. Verstraete, M. M. Wolf, and J. I. Cirac, *Quantum Inf. Comput.* **7**, 401 (2007).
 [S5] S. R. White, *Phys. Rev. Lett.* **69**, 2863 (1992).
 [S6] U. Schollwöck, *Ann. Phys. (Amsterdam)* **326**, 96 (2011).
 [S7] M. P. Zaletel, R. S. K. Mong, C. Karrasch, J. E. Moore, and F. Pollmann, *Phys. Rev. B* **91**, 165112 (2015).
 [S8] <http://itensor.org>.
 [S9] J. J. Sakurai, *Modern Quantum Mechanics* (Addison-Wesley, Reading, MA, 1994).
 [S10] M. E. Rose, *Elementary Theory of Angular Momentum* (Wiley, New York, 1967).
 [S11] S. Kitamura and H. Aoki, *Phys. Rev. B* **94**, 174503 (2016).
 [S12] A. Rosch, D. Rasch, B. Binz, and M. Vojta, *Phys. Rev. Lett.* **101**, 265301 (2008).
 [S13] J.-S. Bernier, P. Barmettler, D. Poletti, and C. Kollath, *Phys. Rev. A* **87**, 063608 (2013).
 [S14] A. G. Rojo, J. O. Sofo, and C. A. Balseiro, *Phys. Rev. B* **42**, 10241 (1990).
 [S15] J. Mentink, K. Balzer, and M. Eckstein, *Nat. Commun.* **6**, 6708 (2015).